Molecular organization and solution properties of N-substituted aminomethane-1,1-diphosphonic acids†

Ewa Matczak-Jon,*[a] Wanda Sawka-Dobrowolska,[b] Paweł Kafarski[c] and Veneta Videnova-Adrabińska[a]

[a] *Institute of Inorganic Chemistry, Wrocław University of Technology, 50-370 Wrocław, Poland. E-mail: JON@ichn.ch.pwr.wroc.pl*
[b] *Faculty of Chemistry, University of Wrocław, 50-383 Wrocław, Poland*
[c] *Institute of Organic Chemistry, Biochemistry and Biotechnology, Wrocław University of Technology, 50-370 Wrocław, Poland*

Received (in Montpellier, France) 9th March 2001, Accepted 25th July 2001
First published as an Advance Article on the web 23rd October 2001

The crystal structures of *N*-*n*-pentylaminomethane-1,1-diphosphonic (**1**), *N*-pyrrolidinomethane-1,1-diphosphonic (**2**), *N*-(3-carboxy-2-pyridyl)aminomethane-1,1-diphosphonic (**3a**) and *N*-(5-methyl-2-pyridyl)aminomethane-1,1-diphosphonic (**3c**) acids are determined and discussed with respect to their packing patterns and solid state organization. The molecular association and the possible aggregate forms in solution, resulting from the supramolecular features of these materials, are considered. The solution UV and NMR studies are focused on the *N*-2-pyridylaminomethane-1,1-diphosphonic acids **3a**–**e** in order to establish the influence of the structural changes in passing from 3- to 5- or 6-pyridyl substituted aminomethane-1,1-diphosphonic acids on their general complexation properties.

The analogs of the inorganic pyrophosphate that contain a stable, non-hydrolyzable P–C_α–P bond, commonly known as bisphosphonates, have been used for more than twenty years as therapeutic agents for treatment of bone disorders.[1] However, the mechanism of their action still remains unclear. It is interesting that the herbicidal action of these compounds, claimed in the patent literature in 1979,[2] did not received any special attention up to 1995. Several papers dealing with the herbicidal activity and the possible molecular targets for their action renewed the interest in this class of herbicides.[3–7]

In the literature are a number of X-ray structures of bisphosphonates with a side chain amino group positioned away from the central carbon (C_α), in particular, the structures of antiresorptive pamidronate,[8] olpadronate,[9,10] alendronate[11] and neridronate.[12] In sharp contrast to this fact the aminomethane-1,1-diphosphonic acid derivatives remain relatively unexplored and to the best of our knowledge only the crystal structures of *N*,*N*-dimethylaminomethane-1,1-diphosphonic[8,13] and *N*-piperidinomethane-1,1-diphosphonic[14] acids have been reported to date.

The available biochemical data suggest that the herbicidally active aminomethane-1,1-diphosphonic acids should be considered as a heterogeneous group of compounds with various modes of action. Their activity is most likely a result of their simultaneous action on several enzymes that are metal-dependent.[4–7] Recently, we have demonstrated that the capability of the phosphonate groups to form strong hydrogen bonds is not only responsible for their molecular organization in the solid state but also influences the selective metal ion recognition and directs the metal–ligand organization in solution.[15] The ultimate goal of our studies is to elucidate the metal ion binding mechanism of aminomethane-1,1-diphosphonic acids in solution, since it is very likely that the complex-formation abilities of these compounds are of vital importance for their exerted inhibition properties. For that reason the first step of our studies is addressed to the X-ray structure determination of *N*-*n*-pentylaminomethane-1,1-diphosphonic (**1**), *N*-pyrrolidinomethane-1,1-diphosphonic (**2**) and especially of *N*-(3-carboxy-2-pyridyl)aminomethane-1,1-diphosphonic (**3a**) and *N*-(5-methyl-2-pyridyl)aminomethane-1,1-diphosphonic (**3c**) acids, shown in Scheme 1.

On the other hand the solution studies are focused on the group of *N*-2-pyridylaminomethane-1,1-diphosphonic acid derivatives **3a**–**3e** and are aimed at establishing the general complexation features, which are dependent on the topology

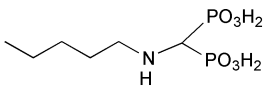

1

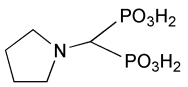

2

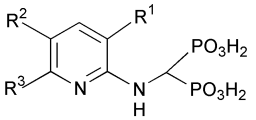

3

	R^1	R^2	R^3
3a	COOH	H	H
3b	CH_3	H	H
3c	H	CH_3	H
3d	H	Cl	H
3e	H	H	CH_3

Scheme 1

† Electronic supplementary information (ESI) available: Tables S1–S3 selected bond lengths and angles for **1**, **2**, **3a** and **3c**. See http://www.rsc.org/suppdata/nj/b1/b102282m/

of the substituents. The solution behavior of **1** and **2** as reflected in their NMR titration curves does not significantly depart from that of the iminodimethylenediphosphonic acids[15] and therefore it will not be discussed in detail.

Experimental

The aminomethane-1,1-diphosphonic acids were obtained according to the previously described procedures.[2,3,16] Their identity was checked using ES-MS spectrometry and their purity was confirmed by their NMR spectra. The $[M + H]^+$ peak for the studied compounds is at *m/z* 262.3 (**1**), 245.1 (**2**), 312.2 (**3a**), 283.2 (**3b**, **3c**, **3e**) and at *m/z* 303.0, 305.1—due to chloride ion ^{35}Cl and ^{37}Cl isotope pattern—for **3d**. It is worth noting that compounds **3a**–**e** are not soluble in organic solvents, poorly soluble in water and only slightly more soluble in alkaline solutions.

Spectroscopic techniques

Mass spectra were recorded in the positive-ion mode on a Finnigan Mat TSQ 700 triple quadrupole mass spectrometer operating with an ESI source. The spray voltage was 4.5 kV and the heated capillary temperature was maintained at 473 K.

The diffuse reflectance spectra of compounds **3a**–**e** were measured from Li_2CO_3 pellets with a Hitachi 365 UV-Vis spectrophotometer and the absorption spectra in water solution at 2×10^{-4} mol dm^{-3} concentration, with a Cary 500 scan UV Vis NIR spectrophotometer.

The NMR spectra were recorded on a Bruker DRX spectrometer operating at 121.50 MHz for ^{31}P, 300.13 MHz for ^{1}H and 75.46 MHz for ^{13}C at 300 K, unless otherwise noted. The chemical shifts are given in relation to 85% H_3PO_4 (^{31}P) and $SiMe_4$. All downfield shifts are denoted as positive. The standard Bruker program was used to perform inverse detected [^{1}H-^{13}C] HMQC experiments that verified the ^{1}H and ^{13}C NMR chemical shift assignments for **3a**–**e**.

The samples for NMR studies were prepared in deuteriated water. The concentration of the ligands was 2×10^{-2} mol dm^{-3} for the ^{1}H, ^{31}P measurements and varied from 5×10^{-2} to 3×10^{-1} mol dm^{-3}, depending upon the sample and the pH, for ^{13}C NMR measurements. Back titrations were performed in the acidic region below pH ~5. The pH was measured using a Radiometer pHM83 instrument equipped with a 2401 C combined electrode and is given as meter readings without correction for pD.

Crystal structure determination

1, **2** and **3a**, **3c** were crystallized from water solutions at room temperature using the slow evaporation method and characterized structurally. Compound **3c** crystallizes very poorly and data collection was done on several different species.

All X-ray diffraction data collections were carried out on a KUMA KM4 CCD four circle diffractometer[17] equipped with an Oxford Cryosystem Cooler using graphite monochromated Mo-Kα radiation, $\lambda = 0.710\,73$ Å. The crystal structures were solved by direct methods using SHELXS97[18] and refined by full-matrix least-squares on F^2 using SHELXL 97.[19] Diffraction data were corrected for Lorentz and polarization effects. All non-H atoms were refined with anisotropic thermal parameters. All H atoms in crystals **1**, **2**, **3a** were located on the difference maps and included in the refinement with isotropic temperature factors. The hydrogens attached to the oxygen and nitrogen atoms in **3c** were found from the difference synthesis and all the remain hydrogens were included in calculated position. The riding model was used for all H atoms and their H atom displacement parameters were fixed at $U_{izo}(H) = 1.2U_{eq}$ or $1.5U_{eq}$(parent). The crystallographic data and experimental details are summarized in Table 1. The computer program PLATON[20] was used to analyze the geometry of the hydrogen-bonding patterns and for graphical representation of the results.

CCDC reference numbers 161070–161073. See http://www.rsc.org/suppdata/nj/b1/b102282m/ for crystallographic data in CIF or other electronic format.

Results and discussion

Solid state organization and hydrogen-bonded networks

The molecular structures and atom numbering of the four crystalline compounds **1**, **2** and **3a**, **3c** are shown in Fig. 1–4. Since the main focus of this paper is concentrated on the supramolecular features of the aminomethane-1,1-diphosphonic acids with respect to their impact on the molecular association in solution, the structural details will not be described

Table 1 Summary of crystal data, data collection and refinement conditions for compounds **1**,**2** and **3a**,**3c**

Compound	**1**	**2**	**3a**	**3c**
Formula	$C_6H_{17}NO_6P_2 \cdot H_2O$	$C_5H_{13}NO_6P_2 \cdot H_2O$	$C_7H_{10}N_2O_8P_2 \cdot H_2O$	$C_7H_{12}N_2O_6P_2$
M	279.16	263.12	330.13	282.13
Crystal system	Monoclinic	Triclinic	Monoclinic	Monoclinic
Space group	$P2_1/c$	$P\bar{1}$	$P2_1/c$	$P2_1$
a/Å	12.374(2)	7.167(1)	11.128(2)	7.313(1)
b/Å	10.334(2)	7.535(1)	8.248(2)	15.940(3)
c/Å	9.428(2)	10.052(2)	13.527(3)	9.421(2)
α/°		98.14(1)		
β/°	92.83(3)	99.10(1)	101.97(3)	97.49(3)
γ/°		99.59(1)		
U/Å	1204.1(4)	520.6(2)	1214.6(5)	1088.8(3)
T/K	100(2)	100(2)	100(2)	100(2)
Z	4	2	4	4
μ(Mo-Kα)/mm^{-1}	0.381	0.436	0.410	0.420
Reflections collected	8337	3652	7865	7790
Independent reflections	2894	2339	2855	5001
R_{int}	0.0635	0.0238	0.0421	refined on all
Final *R* indices [$I > 2\sigma(I)$]				
R_1 [a]	0.0363	0.0341	0.0438	0.089 (7305)
wR_2 [b]	0.0596	0.0909	0.0925	0.250
All data R_1	0.0731	0.0374	0.0685	0.095
wR_2	0.0596	0.0928	0.0983	0.254

[a] $R_1 = \Sigma(F_o - F_c)/\Sigma F_o$. [b] $wR_2 = \{\Sigma[w(F_o^2 - F_c^2)^2]/\Sigma[w(F_o^2)^2]\}^{1/2}$.

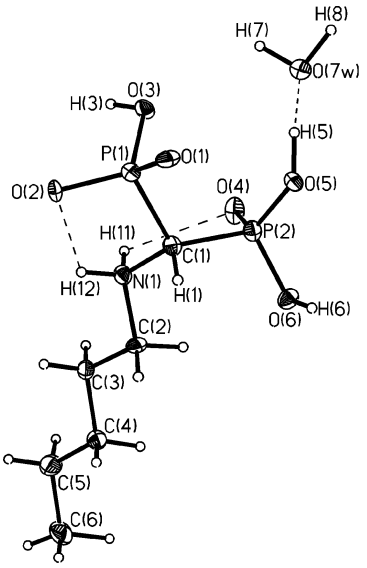

Fig. 1 The molecular structure and the numbering scheme of *N*-*n*-pentylaminomethane-1,1-diphosphonic acid (**1**). Displacement ellipsoids are shown at the 50% probability level (ORTEP II[21]).

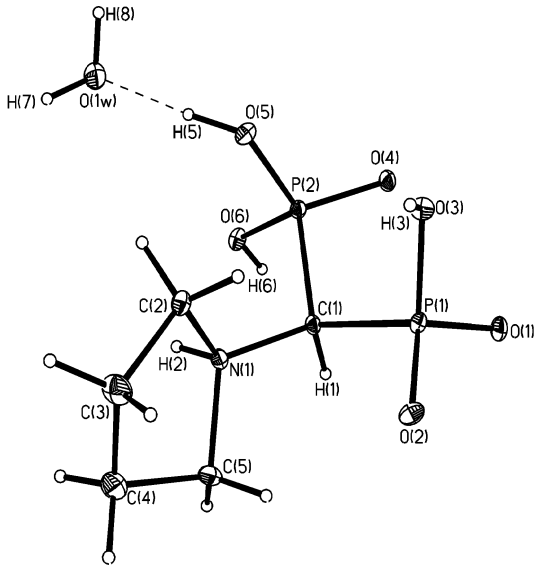

Fig. 2 The molecular structure and the numbering scheme of *N*-pyrrolidinomethane-1,1-diphosphonic acid (**2**). Displacement ellipsoids are shown at the 40% probability level (ORTEP II[21]).

here. All four compounds demonstrate a zwitterionic form with a proton transferred from one of the phosphonic groups to the amino nitrogen N(1) atom in **1** and **2** and to the pyridine nitrogen N(2) in crystals **3a** and **3c**. The zwitterionic form is a common phenomenon for the aminopolyphosphonic acids.[8,9,11–15] Some important structural parameters are collected in Table 2 (see also Tables S1–S3). The only proton, H(3), of the phosphonate $P(1)O_3H^-$ is localized close to the O(3), whereas the two protons in the phosphonic group $P(2)O_3H_2$ are near to O(5) and O(6). So, the P(1)–O(3), P(2)–O(5) and P(2)–O(6) are considered as single bonds. The P–O distances allow the P(1)–O(1) and P(1)–O(2) bonds to be classified as intermediate with a delocalized negative charge in between, whereas P(2)–O(4) is a formal double bond. The bond angular relations (Table 2) in both the phosphonic and the phosphonate groups deviate significantly from the regular tetrahedron that is consistent with the observations in other diphosphonic acids.[8–15] The nearly planar W configuration of the O(2), P(1), C(1), P(2), O(6) atoms appears to be a common feature for all structures. The geometrical parameters of the

Table 2 Selected intramolecular bond lengths (Å), angles (°) and torsion angles (°) for compounds **1**, **2** and **3a**, **3c**

				3c	
	1	**2**	**3a**	Molecule A	Molecule B
P(1)–O(1)	1.502(2)	1.506(1)	1.502(2)	1.472(6)	1.490(6)
P(1)–O(2)	1.497(2)	1.499(1)	1.507(2)	1.511(6)	1.505(6)
P(1)–O(3)	1.566(2)	1.566(1)	1.561(2)	1.546(6)	1.578(6)
P(1)–C(1)	1.825(3)	1.847(2)	1.837(2)	1.836(7)	1.814(7)
P(2)–O(4)	1.478(2)	1.491(1)	1.493(2)	1.497(5)	1.478(6)
P(2)–O(5)	1.523(2)	1.511(1)	1.541(2)	1.541(6)	1.528(6)
P(2)–O(6)	1.556(2)	1.577(1)	1.542(2)	1.558(6)	1.540(6)
P(2)–C(1)	1.834(3)	1.841(2)	1.823(2)	1.817(8)	1.809(8)
N(1)–C(1)	1.512(3)	1.514(2)	1.460(3)	1.432(10)	1.453(10)
N(1)–C(2)	1.516(3)	1.531(2)	1.338(3)	1.341(10)	1.379(10)
O(1)–P(1)–O(2)	116.6(1)	116.3(1)	116.7(1)	114.6(4)	118.3(4)
O(1)–P(1)–O(3)	107.7(1)	107.4(1)	112.5(1)	110.0(4)	109.5(4)
O(2)–P(1)–O(3)	112.2(1)	112.2(1)	108.3(1)	111.0(3)	109.6(3)
O(1)–P(1)–C(1)	107.1(1)	104.2(1)	108.3(1)	111.8(4)	108.6(4)
O(2)–P(1)–C(1)	104.7(1)	109.3(1)	106.5(1)	104.9(3)	104.2(3)
O(3)–P(1)–C(1)	108.1(1)	106.9(1)	103.5(1)	104.0(3)	105.9(4)
O(4)–P(2)–O(5)	118.2(1)	117.1(1)	114.4(1)	117.9(4)	116.4(3)
O(4)–P(2)–O(6)	110.5(1)	111.7(1)	114.5(1)	112.4(3)	114.4(3)
O(5)–P(2)–O(6)	109.4(1)	107.2(1)	106.4(1)	108.3(4)	106.5(3)
O(4)–P(2)–C(1)	106.4(1)	107.2(1)	110.8(1)	110.2(3)	110.5(4)
O(5)–P(2)–C(1)	106.0(1)	108.4(1)	104.8(1)	104.2(3)	105.7(3)
O(6)–P(2)–C(1)	105.5(1)	104.5(1)	105.1(1)	102.5(3)	102.0(3)
P(1)–C(1)–P(2)	117.3(2)	112.9(1)	115.2(1)	117.1(4)	117.4(4)
P(1)–C(1)–N(1)	108.1(2)	115.5(1)	107.4(2)	109.1(5)	109.3(5)
P(2)–C(1)–N(1)	110.9(2)	110.4(1)	109.5(2)	108.8(5)	107.9(5)
C(1)–N(1)–C(2)	113.9(2)	116.8(1)	128.0(2)	124.7(7)	127.2(7)
O(2)–P(1)–C(1)–P(2)	157.8(1)	161.5(1)	−177.0(1)	172.5(4)	−172.6(5)
P(1)–C(1)–P(2)–O(6)	154.1(1)	163.3(1)	−168.2(1)	171.2(5)	−171.9(5)
H(2)–N(1)–C(2)–N(2)			176(2)	4.0	4.4

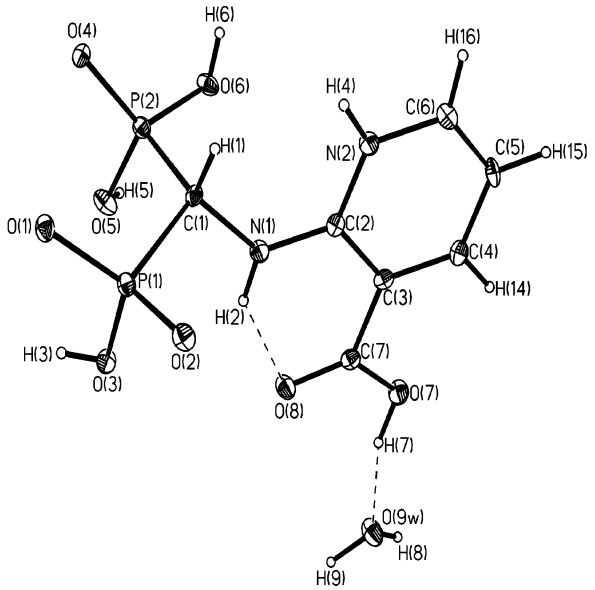

Fig. 3 The molecular structure and the numbering scheme of *N*-(3-carboxy-2-pyridyl)aminomethane-1,1-diphosphonic acid (**3a**). Displacement ellipsoids are shown at the 40% probability level (ORTEP II[21]).

hydrogen bonds are presented in Table 3 with respect to their priorities in the organization of well-defined structural motifs.

The crystalline edifice of 1. The hydrogen-bond directional features combined with the geometrical requirements and the steric confinements in the solid state allow only a phosphonate–phosphonate or phosphonic–phosphonic intermolecular recognition in **1**. The three strongest hydrogen-bond interactions, O(6)–H(6)···O(4) (1), O3–H(3)···O(1) (2) and N(1)–H(11)···O(5) (3) are used between glide-related molecules to form molecular ribbons along the *a* axis (see Fig. 5 and Table 3). The proton transfer from the phosphonic group to the amino N(1) atom in the zwitterion **1** seems to be crucial for the internal molecular configuration since it enables the formation of two intramolecular hydrogen bonds, N(1)–H(12)···O(2) (7) and N(1)–H(11)···O(4) (8), donated toward the formally double bonded phosphonate and the phosphonic

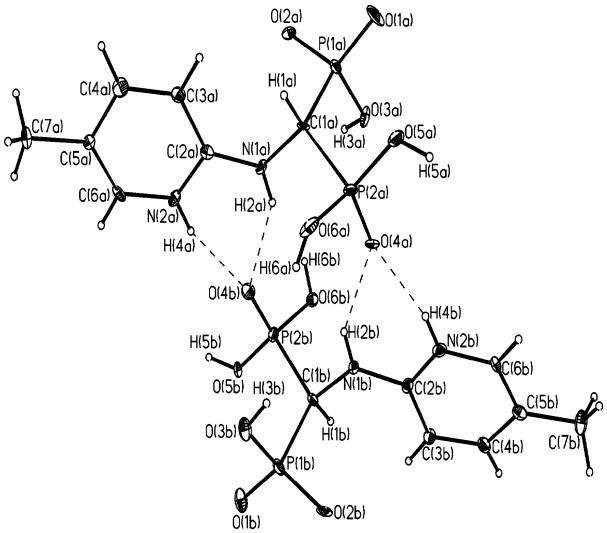

Fig. 4 The molecular structure of the two *N*-(5-methyl-2-pyridyl) aminomethane-1,1-diphosphonic acid (**3c**) molecules in the asymmetric unit, showing the numbering scheme. Displacement ellipsoids are at the 30% probability level (ORTEP II[21]).

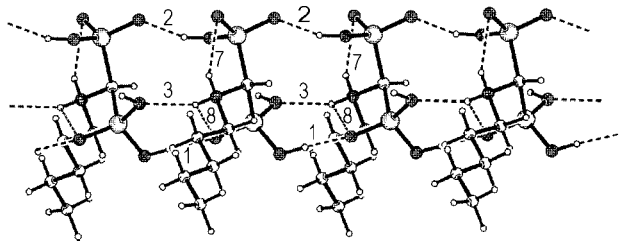

Fig. 5 The molecular ribbons along *c* in **1** are formed by glide-related molecules interlinked *via* three hydrogen-bonds numbered 1, 2, 3, consistent with those in Table 3.

oxygens. This 'freezes' the molecular conformation around the N(1)–C(1), C(1)–P(1) and C(1)–P(2) bonds. An additional intramolecular hydrogen bond, C(2)–H(22)···O(6) (9), stabilizes the nearly planar W configuration of the O(2), P(1), C(1), P(2), O(6) atoms with torsion angles O(2)–P(1)–C(1)–P(2) and P(1)–C(1)–P(2)–O(6) of 157.8(1) and 154.1(1)°, respectively, which appear to be important for the extended network organization. The incorporation of the water molecule in the crystal lattice appears to be indispensable in order to satisfy the free hydrogen bond donor H(5). In fact, the O(5)–H(5)···O(7W) (4) bond forming the crystallographic chemical unit (CCU)[22] is the strongest in the whole crystal network. The water molecules serving as a molecular glue organize the inversion related ribbons into puckered (100) layers *via* O(7W)–H(7)···O(2) (5) and O(7W)–H(8)···O(1) (6) hydrogen bonds whereas the side chains are interdigitatively arranged between those layers. So, the overall crystal structure of **1** comprises well expressed hydrophilic regions of the aminomethane-1,1-diphosphonic portions and hydrophobic regions of the side chains.

The crystalline edifice of 2. Similar to **1**, the zwitterion **2** is formed *via* protonation of the amino nitrogen N(1) atom. The conformaton of the pyrrolidine ring incorporating the N(1) atom is strongly influenced by the methane-1,1-diphosphonic portion. The ring puckering analysis reveals that the pyrrolidine ring is non-planar, adopting a conformation between an envelope and a half-chair with puckering parameters $Q = 0.399(2)$ Å and $\Phi = 313.5(3)°$.[23] In contrast to **1**, the molecular conformation in **2** resulting from the involvement of the N(1) nitrogen in the five-membered ring disfavors the formation of intramolecular hydrogen bonds except for the weak C(5)–H(51)···O(2) (8), which 'freezes' only the rotation of the phosphonic but not of the phosphonate group. This allows for both phosphonic–phosphonate and phosphonate–phosphonate intermolecular hydrogen-bond interactions. The strongest interaction, O(6)–H(6)···O(1) (1), is used to doubly associate inversion related molecules in order to form dimers *via* a big twelve-membered ring motif R2,2(12). The second strongest interaction, O(3)–H(3)···O(2) (2), extends the dimers into molecular ribbons running along the *c* crystallographic axis with subsequent R2,2(8) ring formation (see Fig. 6). The N(1)–H(2)···O(6) (3) bond cross-links the translation related ribbons along the *b* axis in order to form puckered (100) monolayers with the side chains arranged in-between. Similar as in **1**, the water molecule is incorporated in the crystal lattice not only as a space filling agent but also as an interaction-mediating agent between the layers. So, O(1W) is approached by H(5) in order to form the shortest hydrogen bond in the whole system *via* the very strong O(5)–H(5)···O(1W) (4) hydrogen bond. The specific function of the water molecule serving as a triple hydrogen bond donor is reflected in its molecular geometry, demonstrating an almost rectangular configuration with different bond lengths. The H(7) atom serves as a bifurcated hydrogen bond donor toward

Table 3 Hydrogen-bond geometries and hydrogen-bond patterns of compounds **1**,**2** and **3a**, **3c**

	Hydrogen-bond interactions	D···A/Å	D–H/Å	H···A/Å	∠DHA/°	Symmetry code	H bond motif	
	N-*n*-Pentylaminomethane-1,1-diphosphonic acid (**1**)							
	Intermolecular acid–acid H. bonds	Ribbon formation along *c* axis				*c* glide		
1	O(6)–H(6)···O(4)	2.541(2)	0.89(2)	1.65(3)	178(3)	$x, \frac{1}{2}-y, -\frac{1}{2}+z$	C1,1(4)	R2,2(12)
2	O(3)–H(3)···O(1)	2.566(3)	0.92(3)	1.68(3)	159(3)	$x, \frac{1}{2}-y, \frac{1}{2}+z$	C1,1(4)	
3	N(1)–H(11)···O(5)	2.852(3)	0.90(3)	2.01(3)	155(3)	$x, \frac{1}{2}-y, \frac{1}{2}+z$	C1,1(5)	
	Intermolecular acid–water H. bonds	(100) puckered layer formation				Inversion		
4	O(5)–H(5)···O(7W)	2.448(3)	1.06(4)	1.39(4)	176(3)	x, y, z	D	
5	O(7W)–H(7)···O(2)	2.541(3)	1.03(4)	1.52(4)	170(3)	$1-x, \frac{1}{2}+y, \frac{1}{2}-z$	D	R2,2(6)
6	O(7W)–H(8)···O(1)	2.586(3)	1.08(3)	1.57(4)	153(3)	$1-x, -y, -z$	D	
	Stabilizing intramol. H. bonds							
7	N(1)–H(12)···O(2)	2.788(3)	0.91(3)	2.23(3)	120(3)	x, y, z	S1,1(5)	
8	N(1)–H(11)···O(4)	2.929(3)	0.90(3)	2.49(3)	111(3)	x, y, z	S1,1(5)	
9	C(2)–H(22)···O(6)	3.249(3)	1.02(3)	2.49(3)	131(2)	x, y, z	S1,1(5)	
10	C(1)–H(1)···O(2)	2.37(2)	0.92(2)	3.201(3)	150(2)	$1-x, -y, -z$	C(4)	
	N-Pyrrolidinomethane-1,1-diphosphonic acid (**2**)							
	Acid–acid interactions	Acid tapes along *c* axis				Inversion		
1	O(6)–H(6)···O(1)	2.484(2)	0.79(4)	1.70(4)	170(4)	$1-x, 1-y, -z$	R2,2(12)	C2,2(10)
2	O(3)–H(3)···O(2)	2.529(2)	0.79(3)	1.74(3)	178(3)	$1-x, 1-y, 1-z$	R2,2(8)	
	Acid–acid interactions	2D acid network-(100) puckered layers				Translation along *b*		
3	N(1)–H(2)···O(6)	2.869(2)	0.88(3)	2.01(3)	163(2)	$1-x, -y, -z$	R2,2(10)	
	Acid–water interactions	3D network				Translation along *a*		
4	O(5)–H(5)···O(1W)	2.431(2)	0.94(6)	1.50(6)	168(5)	x, y, z	D R4,4(12)	R2,4(8)
5	O(1W)–H(8)···O(4)	2.563(2)	0.92(5)	1.91(5)	126(4)	$-x, -y, -z$	D R4,4(12)	
6	O(1W)–H(7)···O(4)	2.991(2)	0.93(4)	2.59(4)	107(3)	$x, -1+y, z$	D R2,1(6)	
7	O(1W)–H(7)···O(1)	2.622(2)	0.93(4)	1.74(4)	156(4)	$x, -1+y, z$	D R2,1(6)	
	Stabilizing interactions							
8	C(5)–H(51)···O(2)	3.116(2)	0.94(3)	2.35(3)	139(2)	x, y, z	S1,1(6)	
9	C(5)–H(52)···O(1W)	3.348(3)	0.94(3)	2.56(3)	141(2)	$1-x, -y, -z$	D	
10	C(2)–H(22)···O(1)	3.364(2)	0.97(3)	2.54(3)	144(2)	$x, -1+y, z$	C1,1(4)	
11	C(1)–H(1)···O(4)	3.477(3)	0.95(2)	2.55(2)	166(2)	$1-x, 1-y, -z$	C1,1(4)	
12	C(4)–H(42)···O(2)	3.547(2)	0.97(3)	2.60(3)	167(2)	$2-x, 1-y, 1-z$	C1,1(4)	
	N-(3-Carboxy-2-pyridyl)aminomethane-1,1-diphosphonic acid (**3a**)							
	Acid–acid interactions	Helical tapes along *b* axis				Screw rotation along *b*		
1	O(6)–H(6)···O(1)	2.497(3)	0.81(5)	1.69(5)	170(4)	$-x, -\frac{1}{2}+y, \frac{1}{2}-z$	C1,1(6)	R2,2(8)
2	O(3)–H(3)···O(4)	2.639(3)	0.81(3)	1.83(3)	172(3)	$-x, \frac{1}{2}+y, \frac{1}{2}-z$	C1,1(6)	
3	N(2)–H(4)···O(4)	2.740(3)	0.81(4)	2.00(4)	152(4)	$-x, -\frac{1}{2}+y, \frac{1}{2}-z$	D	
		2D acid network-(100) puckered layers				*c* glide		
4	O(5)–H(5)···O(2)	2.501(2)	0.82(4)	1.69(4)	170(4)	$x, \frac{1}{2}-y, \frac{1}{2}+z$	C1,1(6)	
	Acid–water interactions	3D network				Translation along *a*		
5	O(7)–H(7)···O(9W)	2.519(3)	0.93(4)	1.62(4)	161(3)	x, y, z	D	
6	O(9W)–H(9)···O(2)	2.668(3)	0.98(4)	1.71(4)	166(3)	$1-x, \frac{1}{2}+y, \frac{1}{2}-z$	D	
7	O(9W)–H(8)···O(1)	2.757(3)	0.70(3)	2.06(4)	176(4)	$1+x, \frac{1}{2}-y, \frac{1}{2}+z$	D	
	Stabilizing interactions							
8	N(1)–H(2)···O(8)	2.660(3)	0.87(3)	1.94(3)	139(2)	x, y, z	S1,1(6)	
9	N(1)–H(2)···O(3)	2.948(2)	0.87(3)	2.55(3)	108(2)	x, y, z	S1,1(5)	
10	C(4)–H(14)···O2	3.340(3)	0.99(3)	2.51(3)	141(2)	$1-x, -\frac{1}{2}+y, \frac{1}{2}-z$		
	N-(5-Methyl-2-pyridyl)aminomethane-1,1-diphosphonic acid (**3c**)							
	Intradimer H. bond interactions	A–B dimeric units				Screw rotation $2_1(y)$		
1	O(5A)–H(5A)···O(1B)	2.442(8)	0.83	1.85	127	$1-x, \frac{1}{2}+y, -z$	D	
2	O(5B)–H(5B)···O(1A)	2.447(8)	0.82	1.74	143	$-x, -\frac{1}{2}+y, -z$	D	R3,3(14)
	Interdimer H. bond interactions	A–B ribbons along *a* axis				Translation along *x* axis		
3	O(6B)–H(6B)···O(2B)	2.553(8)	0.83	1.77	156	$-1+x, y, z$	C1,1(6)	
4	O(6A)–H(6A)···O(2A)	2.658(8)	0.82	1.95	144	$1+x, y, z$	C1,1(6)	
	Inter-ribbon H. bond interactions	(001) puckered layers						
5	O(3B)–H(3B)···O(2A)	2.567(8)	0.83	1.82	149	$1+x, y, z$	D	
6	O(3A)–H(3A)···O(2B)	2.620(9)	0.82	1.83	163	$-1+x, y, z$	D	
7	N(2B)–H(4B)···O(4A)	2.644(9)	0.86	1.86	151	x, y, z	D	R1,2(6)
8	N(1B)–H(2B)···O(4A)	2.827(8)	0.87	2.07	145	x, y, z	D	
9	N(2A)–H(4A)···O(4B)	2.695(9)	0.87	1.90	152	x, y, z	D	R1,2(6)
10	N(1A)–H(2A)···O(4B)	2.848(9)	0.86	2.10	145	x, y, z	D	
	Stabilizing interactions							
11	C(6B)–H(16B)···O(3B)	3.179(10)	0.93	2.27	167	$-x, -\frac{1}{2}+y, -z$		
12	C(6A)–H(16A)···O(3A)	3.215(9)	0.93	2.31	165	$1-x, \frac{1}{2}+y, -z$		

two oxygen atoms located on the phosphonic and the phosphonate groups of the same molecule, thus forming the six-membered ring motif R2,1(6) *via* O(1W)–H(7)···O(4) (6) and O(1W)–H(7)···O(1) (7). On the other hand, the (100) monolayers are interwoven by the very strong O(1W)–H(8)···O(4) (5) hydrogen bond. Generally, the pyrrolidine rings are embedded in the big hydrophobic chambers formed between the hydrogen-bonded monolayers.

The crystalline edifices of 3a and 3c. The replacement of the aliphatic side chain by a heteroaromatic ring leads to significant changes in both the molecular configuration and in the

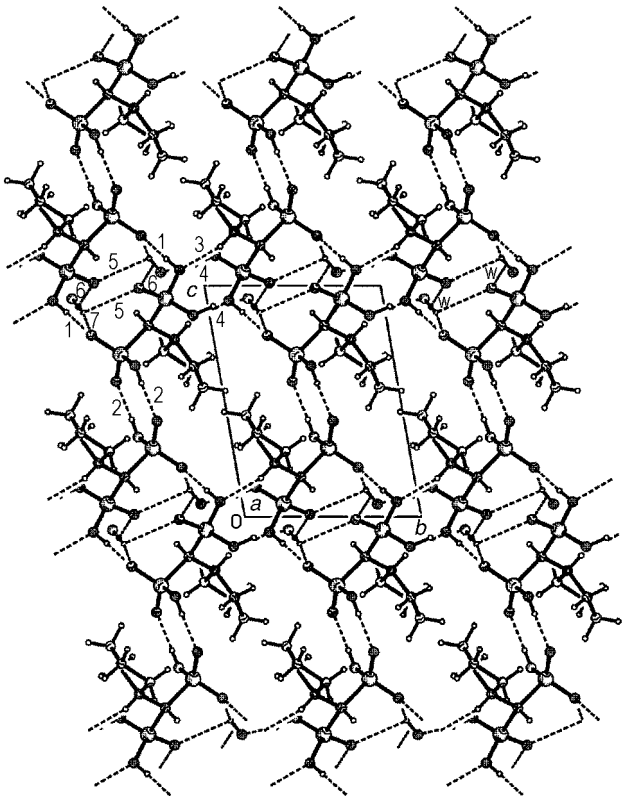

Fig. 6 The hydrogen-bonded molecular layers (*bc*) in **2** formed *via* acid–acid interactions 1, 2, 3. The water molecules occupying positions between the layers are protruding into the twelve-membered ring motifs formed between phosphonate and phosphonic parts of close inversion-related molecules. The side chains are embedded in hydrophobic chambers formed between the layers and protrude into the large holes in the layers [hydrogen-bonded motif R6,6(22) constituted by 1, 2, 3]. The numbers assigned to the hydrogen-bond interactions are consistent with those in Table 3.

molecular organization. The proton transfer toward the pyridine instead of to the amino nitrogen does not substantially change the ring geometry, but the consequences for the molecular configuration are significant. In marked contrast to compounds **1** and **2**, where the amino nitrogen atom forms chemically equivalent bonds with the carbon atoms around it, the pyridine ring attached directly to the amino nitrogen strongly influences the geometry of the N(1)–C(2) and N(1)–C(1) bonds in **3a** and **3c**. Due to the conjugation between the lone pair on the amino nitrogen and the electron deficient heteroaromatic ring, the N(1)–C(2) bond bears partial double bond character and is significantly shortened (see Table 2). A similar relation is observed also for other 2-aminopyridine derivatives.[24] The free rotation of the aminomethane-1,1-diphosphonic portion becomes hampered and only librational motions around the N(1)–C(2) bond are allowed. The C(1)–N(1) bond tends to align co-planar with the pyridine ring (forming angles with the least square ring planes of 5.4° in **3a**, and 6.1 and 4.0° in the A and B molecules of **3c**).

Compounds **3a** and **3c** demonstrate two different conformations around the N(1)–C(2) bond [see the torsion angles H(2)–N(1)–C(2)–N(2) in Table 2]. In **3a** the exocyclic NH proton assumes an *E* orientation with respect to the pyridine nitrogen (*E* isomer) whereas in **3c,** if the same notation, is used the *Z* orientation is preferred (*Z* isomer). The carboxylic group in the position C-3 seems to be crucial for the internal molecular configuration since it is located close to the amino group. The amino hydrogen atom H(2) adopts an *E* orientation in order to approach the lone pair on the carbonyl oxygen O(8), forming a N(1)–H(2)···O(8) (8) hydrogen bond with a ring motif S(6). The self-association 'freezes' the rotation around the C(3)–C(7) bond and arranges both the amino and the carboxylic groups almost co-planar with the pyridine ring. The three-dimensional network is substantially dictated by the hydrogen-bond donor and acceptor capability of the phosphonic group since it is the only molecular portion that is not rotationally restrained. The screw-related molecules are extended *via* O(6)–H(6)···O(1) (1) and O(3)–H(3)···O(4) (2) in order to form helical chains along the *b* axis [Fig. 7(a)]. The second lone pair on the phosphonate O(4) oxygen is additionally accessed by the pyridine H(4) atom in order to form the N(2)–H(4)···O(4) (3) bond, which congeals the molecular scaffold with the methane-1,1-diphosphonic portions hidden inside the helices and the aromatic rings arranged from the outside. Only the phosphonate O(2) atom is accessible for an inter-chain hydrogen bond donated from the H(5) atom, which protrudes from the helical loops. So, the second strongest interaction O(5)–H(5)···O(2) (4) is used to associate the inversion-related helical chains into puckered (100) layers, generating large chambers in-between. The water molecule is incorporated in the crystal lattice to satisfy both hydrogen bond and dense packing demands, forming three strong acid–water interactions, O(7)–H(7)···O(9W) (5), O(9W)–H(9)···O(2) (6) and O(9W)–H(8)···O(1) (7) that associate the layers in the third direction and complete the crystal framework [Fig. 7(b)].

Compound **3c** crystallizes in a non-centrosymmetric space group with two independent molecules A and B in the asymmetric unit cell. The strongest hydrogen bond interactions, O(5A)–H(5A)···O(1B) (1) and O(5B)–H(5B)···O(1A) (2), are used to combine each A molecule with two B molecules or each B to two A molecules in order to form molecular trimers A–B–A and B–A–B. Two other strong interactions, O(6A)–H(6A)···O(2A) (4) O(6B)–H(6B)···O(2B) (3), are used to extend the trimers into molecular ribbons constituted by two independent molecular chains A and B running along the *a* crystallographic direction [Fig. 8(a)]. The next strongest hydrogen bonds, O(3B)–H(3B)···O(2A) (5) and O(3A)–H(3A)···O(2B) (6), associate the ribbons in the second direction in order to form puckered (001) molecular layers. Although both *Z* and *E* conformers are allowed for the one-dimensional arrangement, for synergetic and adaptability reasons, the *Z* conformation is preferred for the two-dimensional hydrogen-bonded network with a subordinated offset face-to-face (OFF) arrangement between the screw-related aromatic rings displaced from both sides of the layers. Exchange van der Waals interactions hold the layers together in the third direction with a resultant alternation of hydrophobic and hydrophilic regions along the *c* axis [Fig. 8(b)].

Assuming that the hydrogen-bond strength (expressed by the O···O distance) is informative for the priorities of hydrogen-bond formation it becomes evident that the molecular trimers B–A–B and/or A–B–A, both forming fourteen-membered ring motifs R3,3(14), can be considered as the smallest modular units that build the three-dimensional network *via* simple translations.

Solution studies of compounds 3a–e

The partially double bond character of the exocyclic C–N bond with the resultant almost planar arrangement of the 2-aminopyridine unit, observed in **3a** and **3c**, is dictated by the tendency of these compounds to delocalize their amino lone pair onto the pyridyl ring π system. This general property of all 2-aminopyridine derivatives is conveniently described in terms of resonance between the mesomeric structures **I** and **Ia**[25] (Scheme 2), which additionally suggests an increase in the rotational barrier around the $C–N_{amino}$ bond in solution.

The UV absorption and the reflectance spectra of **3a–e** (Table 4) are compared with those of the parent 2-aminopyridine[26–28] and demonstrate an evident similarity in

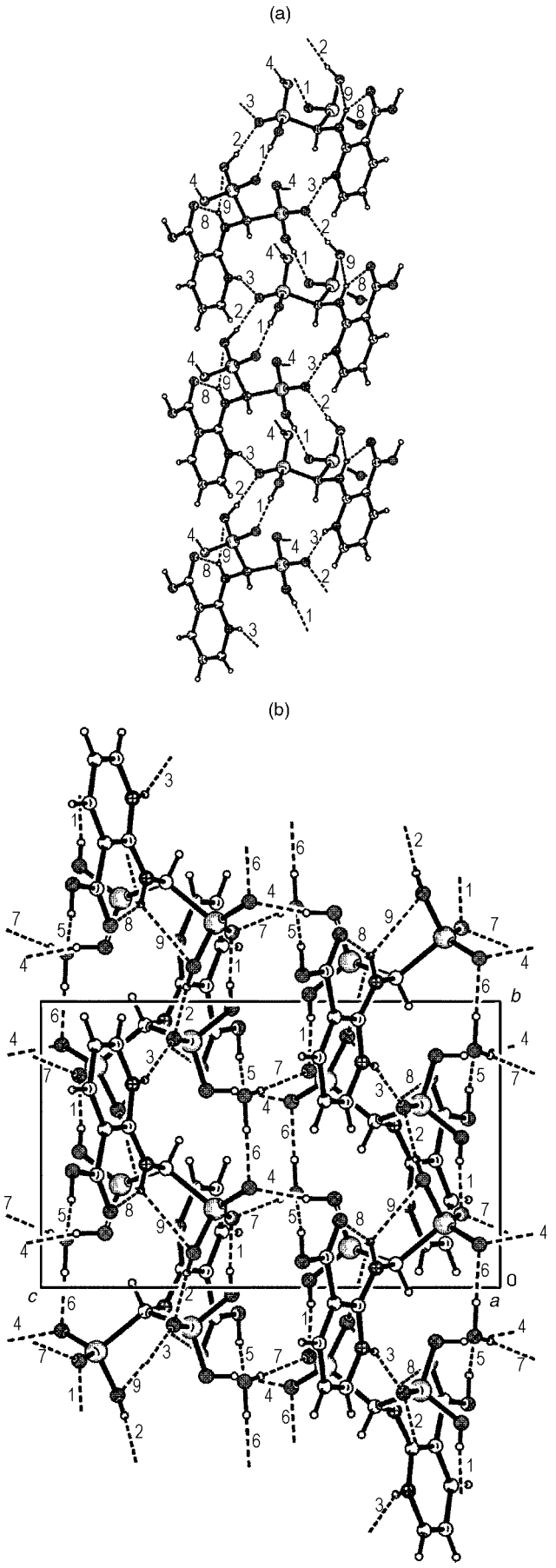

Fig. 7 (a) The helical tapes in **3a** are formed *via* phosphonate–phosphonic (1 and 2) and pyridyl–phosphonate (3) hydrogen bonds. (b) The molecular tapes are interconnected (*via* 4) to form a hydrogen-bonded layer. Water molecules interlink the layers in the third direction (5, 6, 7). The numbers relating to the hydrogen-bond interactions are consistent with those in Table 3.

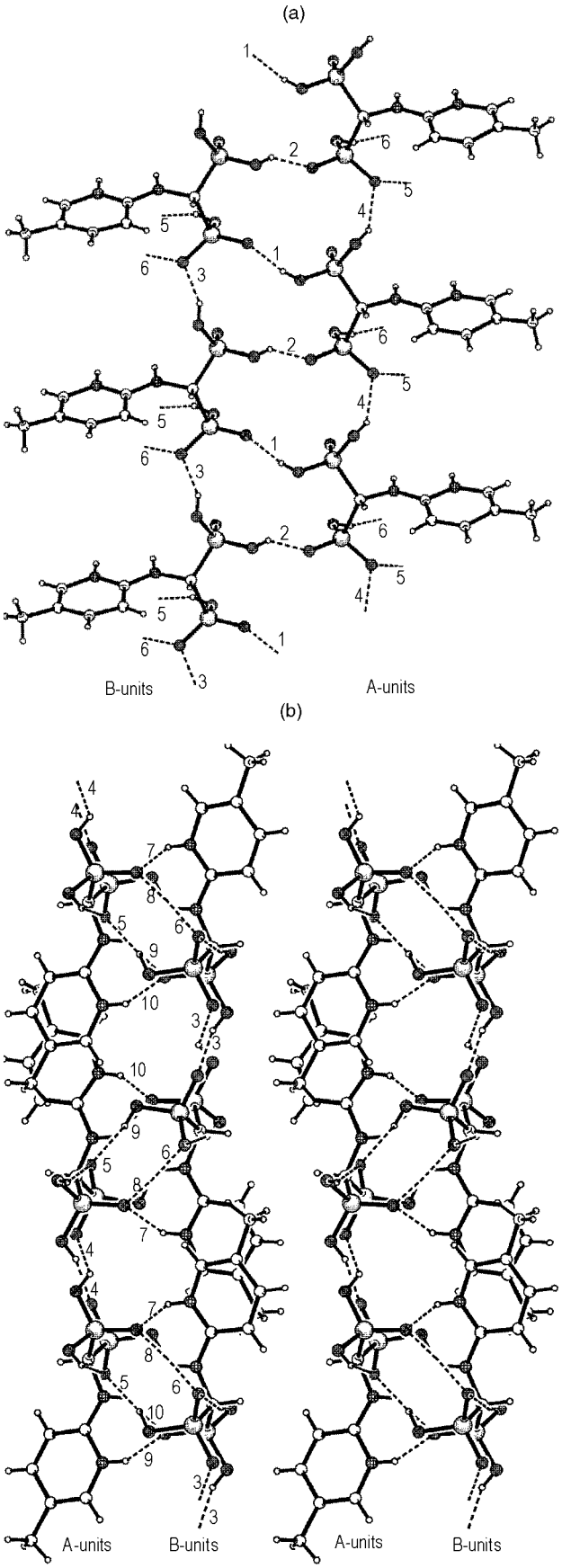

Fig. 8 (a) Representation of the *ab* projection of the one-dimensional network in **3c** consisting of molecular ribbons formed by two molecular chains A and B. (b) The representation of the packing motif projected in the *bc* plane demonstrates the hydrophobic and hydrophilic regions alternating along the *c* axis, as well as the interconnection between the molecular ribbons (*via* 5, 6, 7, 8, 9, 10) in the hydrogen-bonded *ab* monolayers. The numbers relating to the hydrogen-bond interactions are consistent with those in Table 3.

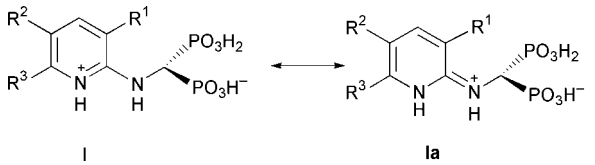

I Ia

Scheme 2

their spectral patterns. This indicates that the conjugation of the lone pair of the amino nitrogen with the pyridine ring mainly accounts for the electronic properties in both the crystalline and the aqueous solution state. The two broad absorption bands observed in the spectra of **3a–e** presumably can be interpreted as π–π^* transitions. The band position shift toward the longer wavelengths with respect to the bands observed in 2-aminopyridine (Table 4) reflects the presence of additional phosphonate functionalities. Upon increasing the pH in solution all compounds exhibit a spectral behavior similar to that demonstrated in the representative spectra of **3b** (Fig. 9). The shorter wavelength band gains in intensity and shifts batochromically with pH, whereas that at longer wavelength decreases in intensity while changing its position only slightly.

In order to comprehend the conformational preferences and the possible tautomeric exchange properties of compounds **3a–e** their NMR spectra have been monitored over a wide range of pH. The spectral behavior has been carefully studied with respect to the electronic and steric effects of the pyridine substituents. The proton and the carbon NMR spectra assignments are presented in Table 5. A single set of resonances is displayed in both the ^{1}H and the ^{13}C NMR spectra at 300 K.

Table 4 UV reflectance and absorption spectral data of compounds **3a–e**

Compound	λ_{max}/nm	
2-Aminopyridine[26]	229	300
3a	263	346
pH = 8.28[a]	258(13 300)	337(4150)
3b	247	319
pH = 7.23[a]	242(10 900)	311(6300)
3c	250	320
pH = 7.29[a]	244(11 080)	325(3745)
3d	257	333
pH = 7.41[a]	254(16 620)	322(3265)
3e	250	335
pH = 7.38[a]	244(12 920)	316(6650)

[a] Dissolved in H_2O, the values in parentheses are ε_{max} (dm^3 cm^{-1} mol^{-1}).

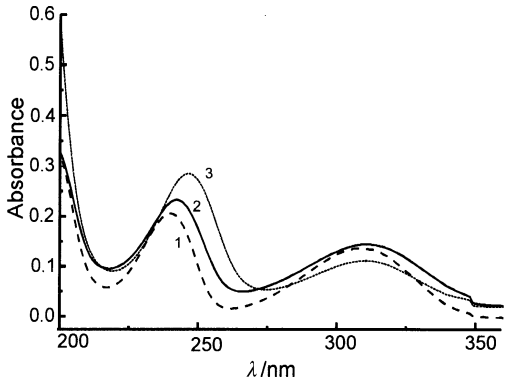

Fig. 9 The UV absorption spectra of **3b** in H_2O at pH 3.50 (1), 7.23 (2) and 11.22 (3).

An exception appears to be the C-2 carbon, for which two separate ^{13}C resonances are detected for **3a**, **3b** in alkaline conditions**.** The new resonance line attributed to C-2 is less apparent for **3d** and it is not observed at all in **3c** and **3e**. The relevant ^{31}P NMR spectra display only one signal for both phosphonate groups over the whole range of pH studied. In addition, the position of the C-3 carbon resonance can serve as a rough estimation of the conjugation enforcing the planarity of the 2-aminopyridine unit.[29] In all protonation states the C-3 resonances of **3c**, **3d** and **3e** are found at chemical shift values that are characteristic for a planar geometry of 2-aminopyridine [δ(C-3)$_{D_2O}$ = 110.8 ppm].[28] Due to the additional inductive and steric effects of the substituent in **3a** and **3b** the C-3 chemical shift in these compounds is not very informative. However, the existence of similar conjugation has already been proved by the structural analysis (see Fig. 3, Table 2) and by the UV spectra (Table 4).

It is well established that the deprotonation of functional groups like PO_3H^- or NH_3^+ shifts the signals of the neighboring proton(s) upfield compared to those of the protonated ligand forms.[30] Consequently, the methine proton resonance, appearing as a triplet in the ^{1}H NMR spectra of **1** and **2**, shifts gradually upfield with increasing pH. Generally, this tendency is observed also for the ^{1}H NMR chemical shift profiles of **3c–e**. However, compounds **3a** and **3b** exhibit divergent spectral behavior at pH > 7 [Fig. 10(a)].

On the other hand, the dependence of the ^{31}P chemical shifts upon pH are very similar for all the compounds except **3d** [Fig. 10(b)]. Hence, the respective deprotonation constants for **3c** and **3e** can be assumed to be close to those reported for **3b**[31,32] ($pK_{PO_3H^-}$ = 10.49, $pK_{PO_3H^-}$ = 8.05, pK_{NH^+pyr} = 5.30 and $pK_{PO_3H_2} \approx$ 1–2). The electron-withdrawing carboxylic group (pK_{COOH} = 2.39[32]) in **3a** only slightly increases the

Table 5 Selected ^{13}C and ^{1}H NMR chemical shifts of compounds **3a–e** in D_2O at 300 K

		^{13}C/ppm						^{1}H/ppm				
Compound	pH	C-2[a]	C-3	C-4	C-5	C-6	CH(P_2)[a]	H-3	H-4	H-5	H-6	CH(P_2)[a]
3a	2.91	152.45(4.6)	116.96	138.42	111.98	146.40	51.36(128.8)		8.45	6.85	7.84	4.14(19.3)
	5.56	152.91(4.4)	119.19	137.71	111.73	145.29	51.55(126.8)		8.36	6.79	7.78	4.04(20.1)
	10.67	157.14(3.8) 164.49	114.73	141.05	110.60	148.39	49.94(124.1)		7.92	6.44	7.91	4.41(19.8)
3b	5.42	151.80(3.7)	123.67	132.14	113.07	142.07	52.47(126.2)		7.46	6.77	7.66	4.02(20.1)
	11.04	155.89(3.5) 166.80	119.60	137.88	111.44	141.09	51.68(125.9)		7.25	6.42	7.70	4.11(19.4)
3c	4.94	151.13(4.2)	113.12	145.79	123.25	132.55	51.46(128.2)	6.96	7.67		7.51	3.97(19.9)
	11.39	156.69[b]	108.05	139.96	120.89	144.45	52.29(127.0)	6.51	7.30		7.60	3.68(19.5)
3d	5.77	155.13	111.59	139.51	119.21	141.39	50.53(128.8)	6.70	7.50		7.81	4.15(20.2)
	10.88	157.08 164.91[c]	108.85	137.38	117.70	144.58	51.56(128.8)	6.52	7.36		7.76	3.78(19.3)
3e	5.38	153.08(3.7)	110.03[b]	143.89	112.52	146.88	52.14(126.2)	6.81	7.68	6.60		3.93(20.2)
	11.12	157.55[b]	105.86	139.93	111.26	153.64	51.08(124.5)	6.46	7.39	6.37		3.66(19.3)

[a] Triplet, averaged $J_{P\text{-}C}$ ($J_{P\text{-}H}$) experimental values (Hz) in parentheses. [b] Broadened. [c] Minor intensity.

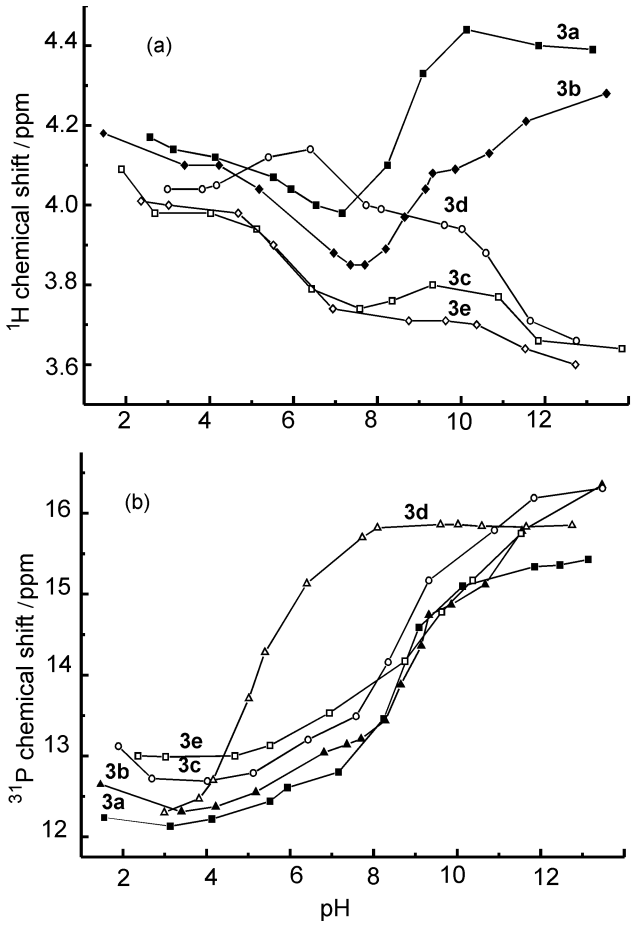

Fig. 10 (a) Methine proton and (b) phosphorus NMR chemical shifts as a function of pH for compounds **3a**–**e**.

pK_{NH^+pyr} and decreases the respective $pK_{PO_3H^-}$ values. The markedly different pH dependence of the ^{31}P titration curve of **3d** is interpreted in terms of reduced basicity of the pyridine NH^+ and the PO_3H^- groups and is attributed to the inductive effect of the electron-attracting chloride substituent of the 5-chloropyridyl ring. This observation is in line with the pH dependent changes in the chemical shifts of the methine proton [Fig. 10(a)] where the inflection points (the middle points of the buffer region) correlate well with the deprotonation constants determined potentiometrically[32] ($pK_{PO_3H^-}$ = 9.69, $pK_{PO_3H^-}$ = 6.52, pK_{NH^+pyr} = 4.67), provided that the conversion of pK_H to pK_D and the changes in temperature and ionic strength are taken into account. Despite these differences the general behavior of the CH proton resonance of **3d**, showing an upfield shift in alkaline solution, is still coherent with those of **3c** and **3e**.

The diverse spectral behavior of the CH proton resonance, observed for **3a** and **3b** at high pH [Fig. 10(a)], is most probably due to their conformational differences *vs.* **3c**–**e**. As already discussed, **3a** and **3c** appear as opposite (*E* and *Z*) isomers in the solid state. Correspondingly, the methine proton in **3a** lies out of the C(1)–N(1)–C(2) plane and the torsion angle H(1)–C(1)–N(1)–C(2) is −29(2)°. So, it appears to be within the vdW distance with the N_{pyr} [H1···H4 = 2.20(8) Å < vdW = 2.40 Å; H1···N2 = 2.68(2) Å < 2.75 Å]. Given the fact that the methine ^{1}H resonances are at downfield positions with respect to those determined for **3c**, a deshielding effect from the pyridine nitrogen can be expected in **3a**. As already discussed the *E* conformation is an intrinsic molecular property of **3a**, preserved also in solution. With increasing pH the intermolecular hydrogen bonds start to break and the conformational constrains on the C(1)–N(1) bond are relaxed. The methine proton tends to align coplanar with the pyridine ring due to the additional repulsion forces experienced between the COO^- and the PO_3^{2-} groups. Therefore, the characteristic downfield shifting of the CH proton signal in **3a**, accompanied by a negative charge gain during the successive deprotonation of the phosphonate groups, may be attributed to the increase of the fractional population of the new conformer. Consequently, the extraordinary downfield shifiting of the CH proton resonance [Fig. 10(a)] is considered as a combination of two effects: the deshielding contributed by the pyridine ring current and the deshielding introduced by the electron lone pair of the deprotonated nitrogen in the proximate pyridine ring. The similar behavior of the CH proton resonance in **3b** allows us to anticipate that the *E* conformer is also preferred in solution. However, the deshielding is less strongly expressed than in **3a** since the repulsion forces between the neutral methyl group and the phosphonic groups are significantly weaker.

In addition the C-2 resonance for both **3a** and **3b** splits ($\Delta\delta \sim 7$ and ~ 10, respectively) at pH higher than 8–9 (*cf.* Table 5). Particularly in the case of the upfield signal, the $^3J_{P\text{-}C}$ coupling constants are very similar in magnitude to those in **1** (3.3 Hz, pH = 13.45) and **2** (2.3 Hz, pH = 13.60). The downfield resonances appear as singlets. It is worth mentioning that this process is fully reversible when pH decreases. A possible explanation of this spectral feature might be a tautomerization involving a proton migration between the amino and pyridine nitrogen sites with a resultant equilibrium between the two conceivable tautomeric forms **II** and **III** (Scheme 3).

Accordingly, the upfield C-2 resonance is undoubtedly attributable to the commonly favored amino tautomer **II** and the downfield signal, detected exclusively in alkaline conditions, can be tentatively ascribed to the imino tautomer **III**. Although the UV spectra of **3a** and **3b** do not confirm such an equilibrium[33] in an obvious manner, the comparative ^{13}C NMR spectra measured at 300 and 350 K seem to be supportive of this presumption. The temperature dependence of the chemical shifts is most apparent in the case of the C-6 and C-2 (upfield) signals. Additionally, the observed differences in the chemical shifts are accompanied by a significant increase in the linewidths of the C-2 resonances at 350 K, which can indicate a dynamic process in the system. Since the appearance of the C-2 (downfield) signal is always correlated with the low-field position of the methine proton, the value of the δ_H chemical shift in the related ^{1}H NMR spectrum can be considered as also being contributed by the tautomer **III**. For reasons of hydrogen bonding the tautomeric form **III** is not possible in the case of **3c**, since the hydrogen bond formed between the amino nitrogen N(1) and phosphonate oxygen O(4) presumably exists even at high pH in solution.

In comparison to **3a** the CH proton in **3c** is much more distant from the nitrogen of the pyridine ring (Fig. 4). On the other hand, the sufficiently remote position of the methyl substituent at C-5 significantly reduces any steric effects. Therefore, two scenarios can be envisaged in solution concerning the single ^{1}H, ^{13}C and ^{31}P resonances detected over the whole studied pH range at 300 K. One possibility is that only the *Z* isomer exists in solution. However, as earlier discussed, there are no stereoelectronic or geometrical reasons for the *Z* form to be preferred. So, the presumption that both *E* and *Z* forms exist in solution seems to be more rational. Each isomeric form yields its own resonance, however, due to the sufficiently fast rotation around the C–N bond only the time-averaged

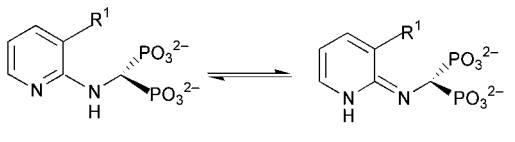

Scheme 3

NMR spectra are detected. This concept seems to find support in the literature data for bis- and tris(dialkylamino)-1,3,5-triazines,[34] where the restricted rotation around the partially double (mean value 1.355 Å) Ar–NH_2 bond was demonstrated to account for the ^1H and ^{13}C NMR spectra at temperatures significantly lower than 293 K. Analogous conclusions can be drawn also for compounds **3d** and **3e**, which behave similarly to **3c**.

Conclusions

In this paper we have shown that X-ray diffraction analysis of the crystalline state, combined with the solution NMR study of N-substituted aminomethane-1,1-diphosphonic acids, can be very useful for revealing the inherent molecular properties of the molecules and their aggregation relations. The perfect molecular organization in hydrogen-bonded networks in the studied crystalline compounds provides valuable information to understand the molecular behavior in solution.

It becomes evident from the crystal structures of **1**–**3a** that the water molecules occupy well-defined sites between multimer hydrogen-bonded molecular formations and play a twofold role. They provide the missing hydrogen-bond donor and acceptor sites for stabilization *via* hydrogen bonding of the three-dimensional frameworks and act as 'space fillers' between these formations. Considering the fact that the basic polymeric (in **1** and **3**) and/or multimeric (in **2**) molecular arrangements in the studied crystals always exploit the two strongest O–H···O hydrogen bonds between the methane-1,1-diphosphonic portions forming resonance-stabilized ring motifs, the presence of some small aggregate forms incorporating the same bonding patterns also seems to be reasonable in solution. Phosphonate–phosphonate and phosphonic–phosphonic bonding is used for one-dimensional polymeric formation in **1**, alternating phosphonic–phosphonate and phosphonate–phosphonate bonding is used in the one-dimensional molecular extensions in **2**, and only phosphonic–phosphonate bonding is used in both the one- and the two-dimensional organization of **3a** (see Table 3 and Fig. 5, 6 and 7). The strongest N–H···O hydrogen bond donated from the protonated amino (**1** and **2**) or pyridine (**3a**) nitrogen is used to additionally stabilize the one-dimensional aggregation in **1** and **3a** or to extend it in a second dimension in **2**. The side groups are arranged in well-expressed hydrophobic regions, efficiently screening the methane-1,1-diphosphonic core and protecting the basic hydrogen-bonded formations from the action of the polar solvent. The above circumstances are to some extent connotative in revealing the complexation process. The metal ion introduced in the solution will gradually replace the phosphonic and phosphonate protons under proper pH conditions with a metal–ligand coordination initiated at the most easy to deprotonate oxygen site. Considering the fact that in crystals **1** and **2** the strongest hydrogen bond is donated from H(5) to the water oxygen and comparing the O–H distances for O(5)–H(5) and O(6)–H(6), it is reasonable to expect that the metal ion coordination should start at O(5) and this should not break the small molecular aggregates (see Fig. 5 and 6) already existing in solutions. Generally, it is impossible to define which proton, H(6) or H(3), will dissociate next upon stepwise increase of pH. However, geometrical considerations allow one to deduce that for steric reasons the metal ion will preferably bind to O(3), thus chelating the two phosphonate groups and forming a six-membered ring. Since the pK values for dissociation of the proton from NRH_2^+(**1**) or $NH_{pyrrolidine}^+$(**2**) are high, a variety of polymeric ligand forms can still be preserved at moderate pH values by O(6)–H(6)···O(4) and N(1)–H(11)···O(5) in **1** and O(6)–H(6)···O(1) and N(1)–H(2)···O(6) in **2**.

In the case of **3a** there is no clear evidence for which hydrogen, H(5) or H(6), will dissociate first. Both hydrogen bonds O(5)–H(5)···O(2) and O(6)–H(6)···O(1) are used in the formation of the basic two-dimensional framework of the ligands. However, due to the mixed phosphonic–phosphonate intermolecular bonding, discrete monomeric complex forms can be expected. No matter where the metal ion coordination will start first, at O(5) or O(6), the metal–ligand binding will destroy the basic hydrogen-bonded network, since the proton H(4) on the pyridine nitrogen is even easier to remove than H(3) and both hydrogen bonds O(3)–H(3)···O(1) and N(2)–H(4)···O(4) will be broken with increasing pH. So, despite the existence of molecular aggregates in pure ligand solution, the coordination of the metal ion will destabilize the whole network, causing gradual breaking of the hydrogen bonds and formation of discrete mononuclear complexes.

Metal ion complex formation in **3c** appears quite different since the energetic priority of the Z isomer for crystal network formation without crystalline water as a hydrogen-bond mediating agent is crucial for its complexation capabilities. The already discussed trimers are probably used as a scaffold for the formation of metal ion complex(es). The details of the complexation mechanism will be discussed in a separate paper. Finally, we have also demonstrated on the examples of **3a**–**e** that the preferred molecular conformation of *N*-2-pyridylaminomethane-1,1-diphosphonic acid derivatives can be established based on the CH proton chemical shift dependence upon pH. In particular, the extraordinary downfield position of the methine resonance can be used as a defining "fingerprint" of the E geometrical isomer.

Acknowledgement

Financial support from The Centre of Nanotechnology and Advanced Materials (project "Non-covalent synthesis. Topochemical control of supramolecular synthesis") is gratefully acknowledged.

References and notes

1 R. Rawls, *Chem. Eng. News*, 1998, **94**, 38; M. J. Rogers, J. C. Frith, S. P. Luckman, F. P. Coxon, H. L. Benford, J. Mönkkönen, S. Auriola, K. M. Chilton and R. G. G. Russell, *Bone*, 1999, **24**, 73S; R. G. G. Russell, P. I. Croucher and M. J. Rogers, *Osteoporosis Int., Suppl.*, 1999, **2**, S66; D. E. Hughes, M. Mian, D. F. Guilland-Cumming and R. G. G. Russell, *Drugs Exp. Clin. Res.*, 1991, **17**, 109.

2 F. Suzuki, Y. Fujikawa, S. Yamamoto, H. Mizutani, T. Ohya, T. Ikai, T. Oguchi, Y. Ochiai and K. Nakahara, *Jpn. Kokai Tokkyo Koho*, 79-37829, 1979; F. Suzuki, Y. Fujikawa, S. Yamamoto, H. Mizutani, T. Ohya, T. Ikai, T. Oguchi, Y. Ochiai and K. Nakahara, *Chem. Abstr.*, 1980, **91**, 103762h; F. Suzuki, Y. Fujikawa, S. Yamamoto, H. Mizutani, C. Funabashi, T. Ohya, T. Ikai and T. Oguchi, *Ger. Offen.*, 28 31 578, 1979.

3 B. Lejczak, B. Boduszek, P. Kafarski, G. Forlani, H. Wojtasek and P. Wieczorek, *J. Plant Growth Regul.*, 1996, **15**, 109; P. Kafarski, B. Lejczak, G. Forlani, R. Gancarz, C. Torreilles, J. Grembecka, A. Ryczek and P. Wieczorek, *J. Plant Growth Regul.*, 1997, **16**, 153; A. L. Chuiko, M. O. Lozinsky, I. Jasicka-Misiak and P. Kafarski, *J. Plant Growth Regul.*, 1999, **18**, 171; G. Forlani, B. Lejczak, P. Kafarski and P. Wieczorek, *J. Plant Growth Regul.*, 1997, **16**, 147.

4 G. Forlani, B. Lejczak and P. Kafarski, *Pestic. Biochem. Physiol.*, 1996, **55**, 180; G. Forlani, B. Lejczak and P. Kafarski, *J. Plant Growth Regul.*, 1999, **18**, 73.

5 T. H. Cromartie, K. J. Fisher and J. N. Grossman, *Pestic. Biochem. Physiol.*, 1999, **63**, 114.

6 V. Oberhauser, J. Gaudin, R. Fonné-Pfister and H.-P. Schär, *Pestic. Biochem. Physiol.*, 1998, **60**, 111.

7 G. Forlani, B. Lejczak and P. Kafarski, *Aust. J. Plant. Physiol.*, 2000, **27**, 667.

8 L. M. Shokol'nikova, S. S. Sotman and E. G. Afonin, *Kristallografiya*, 1990, **35**, 1442.

9 L. M. Shokol'nikova, B. K. Scherbakov, N. M. Dyatlova, T. Y. Medved and M. I. Kabachnik, *Izv. Akad. Nauk SSSr, Ser. Khim.*, 1987, 1511.

10 D. Vega, R. Baggio and O. Piro, *Acta Crystallogr., Sect. C*, 1998, **54**, 324 and references therein.

11 Y. Leroux, D. El Manoui, A. Safaaf, A. Neuman and H. Gillier, *Phosphorus, Sulfur Silicon Relat. Elem.*, 1991, **63**, 181.
12 V. M. Coiro and D. Lamba, *Acta Crystallogr., Sect. C*, 1998, **45**, 446.
13 A. Neels, H. Stoecki-Evans, B. Costissela, H. Jancke, K. D. Knudsen and P. Patison, *Helv. Chim. Acta*, 1999, **82**, 35.
14 M. P. Jensen, J. V. Beitz, R. D. Rogers and K. L. Nash, *J. Chem. Soc., Dalton Trans.*, 2000, 3058.
15 E. Matczak-Jon, B. Kurzak, A. Kamecka, W. Sawka-Dobrowolska and P. Kafarski, *J. Chem. Soc., Dalton Trans.*, 1999, 3627.
16 L. Maier, *Phosphorus, Sulfur Relat. Elem.*, 1981, **11**, 311.
17 Kuma Diffraction KM4CCD™ System Software, v. 1.161, Kuma Diffraction Instruments GmbH, Wrocław, Poland, 1995–1999.
18 G. M. Sheldrick, SHELXL97, Program for Crystal Structure Determination, University of Göttingen, Germany, 1997.
19 A. L. Speck, *Acta Crystallogr., Sect. A*, 1990, **46**, C31.
20 A. L. Speck, PLATON, A Multipurpose Crystallographic Tool, Utrecht University, The Netherlands, 1999.
21 C. K. Johnson, ORTEP II, Report ORNL-5138, Oak Ridge National Laboratory, TN, 1976.
22 The crystal chemical unit (CCU) contains the complete unique molecules and ions that comprise the crystal structure and is synonymous with the asymmetric unit. For more details see: F. H. Allen, O. Kennard, W. D. S. Motherwell, W. G. Town, T. J. Scott and A. C. Larson, *J. Appl. Crystallogr.*, 1974, **7**, 73.
23 D. Cremer and J. A. Pople, *J. Am. Chem. Soc.*, 1995, **97**, 1354.
24 B. C. C. Cantello, D. S. Eggleston, D. Haigh, R. C. Haltiwanger, C. M. Heath, R. M. Hindley, K. R. Jennings, J. T. Sime and S. R. Woroniecki, *J. Chem. Soc., Perkin Trans. 1*, 1994, 3319; C. Bannister, K. Burns, K. Prout, D. J. Watkin, D. G. Cooper, G. J. Durant, C. R. Ganellin, R. J. Ife and G. S. Sach, *Acta Crystallogr., Sect. B*, 1994, **50**, 221.
25 A. R. Katritzky and C. W. Rees, *Comprehensive Heterocyclic Chemistry*, Pergamon Press, Oxford, UK, 1984, vol. 2, part 2A.
26 G. B. Barlin and W. Pheiderer, *J. Chem. Soc. B*, 1971, 1425.
27 S. F. Mason, *J. Chem. Soc.*, 1960, 219.
28 Z. Dega-Szafran, A. Kania, B. Nowak-Wydra and M. Szafran, *J. Mol. Struct.*, 1994, **322**, 223.
29 A. R. Katritzky and J. Ghiviriga, *J. Chem. Soc., Perkin Trans. 2*, 1995, 1651.
30 C. H. Taliaferro and A. A. Martell, *Inorg. Chem.*, 1985, **24**, 2408; E. Matczak-Jon, B. Kurzak, W. Sawka-Dobrowolska, B. Lejczak and P. Kafarski, *J. Chem. Soc., Dalton Trans.*, 1998, 161.
31 B. Boduszek, M. Dyba, M. Jeżowska-Bojczuk, T. Kiss and H. Kozłowski, *J. Chem. Soc., Dalton Trans.*, 1997, 973.
32 B. Kurzak, private communication.
33 K. Inuzuka and A. Fujimoto, *Bull. Chem. Soc. Jpn.*, 1990, **63**, 216; K. Inuzuka and A. Fujimoto, *Bull. Chem. Soc. Jpn.*, 1990, **63**, 971.
34 A. R. Katritzky, D. Oniciu, J. Ghiviriga and R. A. Barcock, *J. Chem. Soc., Perkin Trans. 2*, 1995, 785; A. R. Katritzky, J. Ghiviriga, P. J. Steel and D. C. Oniciu, *J. Chem. Soc., Perkin Trans. 2*, 1996, 443.